PAPER

Significant reduction of cell invasiveness in nanoneedle insertion into a living cell with an electron-beam-deposited probe: impacts of probe geometry, speed and vibration†

Mohammad Shahidul Alam, [ID] [a] Marcos Penedo, [ID] *[b] Takehiko Ichikawa, [ID] [c] Mohammad Mubarak Hosain, [ID] [a] Kyosuke Matsumoto, [ID] [d] Keisuke Miyazawa [ID] [c,d] and Takeshi Fukuma [ID] *[a,c,d]

Intracellular probing of living cells using atomic force microscopy (AFM) has advanced significantly, but it requires specially designed nanoprobes to achieve precision and minimize damage. The development of focused ion beam (FIB)-milled nanoprobes enabled this progress, allowing researchers to fabricate long, sharp probes that penetrate cell membranes with reduced force. Although these FIB-milled probes have been crucial in accessing the intracellular environment, they still cause considerable membrane deformation, limiting their effectiveness in detailed measurements. In response, we developed electron beam deposited (EBD) carbon nanoprobes with varying diameters to further reduce penetration force and resulting cell disturbance. Our study reveals that, for probes of the same diameter, EBD carbon nanoprobes inflict significantly less membrane deformation than FIB-milled ones, due to their sharper tip apex. Additionally, reducing the diameter of the EBD nanoprobes further decreased the penetration force and minimized cell disturbance. We also observed that, at similar speeds, EBD nanoprobes consistently caused less damage, emphasizing the importance of both tip geometry and penetration speed in reducing the impact on cells. Oscillating the cantilever during penetration further reduced friction with the membrane, significantly reducing damage. These findings advance the precision and gentleness of intracellular AFM measurements, offering improved methods for studying cellular mechanics while preserving cell viability.

1. Introduction

Atomic force microscopy (AFM) was first developed for materials research, but its ability to measure biological samples in their natural liquid environment, preserving their native conditions, soon made it an indispensable tool in biological studies. It has broad applications in cell biology, from topographical imaging of individual proteins[1] to entire cells[2] and tissues,[3,4] determining the mechanical properties of cancerous cells[5,6] and detailed imaging of dynamic biological processes.[7] These capabilities contribute to a comprehensive understanding of cellular structures and functions.

AFM cell imaging is not only restricted to examining the cell surface. In recent years, techniques have been developed to directly access the intracellular environments of living cells using a probe typically fabricated on an AFM cantilever, thereby enabling the study of cellular processes in their natural, viable state. For example, the inserted probe can gently extract mRNA from living cells[8,9] without the need for total RNA extraction, thereby minimizing the risk of cell death. To achieve deeper and more precise measurements of intracellular organelles while minimizing cell disturbance, a longer, needle-like AFM nanoprobe can be fabricated by milling the tip equipped with a commercial AFM cantilever using the focused ion beam (FIB) technique. This advanced AFM needle has been effectively used for drug delivery,[10] molecular recognition[11,12] and gene expression analysis.[13] It also facilitates intracellular mechanical studies by enabling direct measurement of the nuclear stiffness in living cells,[14,15]

[a]Division of Nano Life Science, Kanazawa University, Kakuma-machi, Kanazawa 920-1192, Japan. E-mail: fukuma@staff.kanazawa-u.ac.jp
[b]École Polytechnique Fédérale de Lausanne, Institute for Bioengineering, Laboratory for Bio and Nanoinstrumentation, Lausanne CH 1015, Switzerland. E-mail: marcos.penedo@epfl.ch
[c]Nano Life Science Institute (WPI-NanoLSI), Kanazawa University, Kakuma-machi, Kanazawa 920-1192, Japan
[d]Faculty of Frontier Engineering, Kanazawa University, Kakuma-machi, Kanazawa 920-1192, Japan
†Electronic supplementary information (ESI) available. See DOI: https://doi.org/10.1039/d4nr04497e

thereby enhancing our understanding of its role in mechanotransduction. Recently, this technique has been further advanced for intracellular imaging, enabling the direct capture of both 2D and 3D images of internal cell structures, offering unique clarity and depth in the visualization of cellular components in the native state.[16,17]

A key aspect of these intracellular measurements is to minimize cell disturbance, preserving cell behaviour as close to its native state as possible to ensure accurate and reliable imaging data. To achieve this, it is crucial to precisely control both the required force and indentation length of the AFM probe during cell membrane penetration. While a certain amount of force and indentation is inevitable for effective membrane penetration, excessive values can cause serious damage and eventually cell death. In this regard, Nakamura and co-workers conducted several experiments to investigate the impact of needle diameter and tip apex shape on cell membrane penetration.[18,19] They systematically varied these parameters and found that a 200 nm diameter needle with a flat tip apex was the most effective in minimizing cell disturbance.[18] The lack of sharpness in the conical tip apex allowed the flat tip apex to reduce both the force and indentation length by generating higher shear stress on the cell membrane. Our group recently expanded on these studies by fabricating even thinner, conical nanoneedles by FIB.[20] These nanoneedles taper from the base towards the tip, with a diameter of 120 nm at a point 2 μm away from the tip end. The tip itself has a sharp apex with a radius of approximately 50 nm, which further reduces the force and indentation length required for membrane penetration.[20] Although the force needed for penetration was significantly reduced (to around 150 pN) with the use of ultrathin nanoneedles, the indentation length remains relatively large, averaging approximately 700 nm.[20] This poses challenges when working with thinner cells or at the cell periphery, where cell thicknesses could lie below 1 μm. Given the need to reduce the indentation length, we explored reducing the diameter of the nanoneedles to determine whether this approach more effectively minimizes cell disturbance.

Another crucial factor for intracellular measurement is the approaching speed at which the AFM nanoneedle penetrates the cell membrane. Faster approaching speeds can reduce the overall imaging time in intracellular imaging.[16] Previous studies suggest that the optimal approaching speed for nanoneedle penetration ranges from 3 to 10 μm s^{-1}.[21] However, these recommendations were mainly based on the efficiency of membrane penetration, rather than the force or indentation length during penetration. Moreover, Kawamura et al. proposed an optimal speed of 10 μm s^{-1} based on the fishing forces of different intracellular structures in different cell types, which differ from the membrane penetration force.[21] To the best of our knowledge, there has been no systematic experimental study examining how penetration force or indentation length varies with different approaching speeds.

In addition to the challenges mentioned, fabricating AFM nanoneedles for intracellular imaging introduces further complications. Most previous studies[10–20] have consistently utilized nanoneedles fabricated by milling commercial cantilevers using the FIB technique. Although this method allows producing long and relatively sharp nanoneedles, it has a set of drawbacks. The fabrication process for FIB-milled nanoneedles is highly intricate and requires considerable time and skills to execute properly. Fabricating thinner nanoneedles with a diameter of less than 100 nm is challenging, as they often collapse or bend due to mechanical damage during FIB milling.[20] Furthermore, milled nanoneedles often have rough surfaces that can produce unwanted frictions during imaging inside the cells. The peaks in the force versus distance (F–z) curves generated by these frictions often resemble those generated by the tip interaction with intracellular fibers,[16] leading to inaccurate interpretations of acquired data. Additionally, biomolecules from the cellular environment can adhere to the nanoprobe during measurements, requiring the replacement of the cantilever. This prevents us from reusing the same cantilever for routine experiments. Consequently, there is a growing need for more efficient and cost-effective alternatives that can address these limitations while effectively minimizing cell disturbance.

Fabrication of needle-like nanoprobes on AFM cantilevers is not restricted solely to the FIB technique. For instance, the carbon nanoprobe fabricated by the electron beam deposition (EBD) technique has been used for imaging biological molecules under physiological conditions.[22] Shibata et al. employed a longer carbon nanoprobe to image the surface structure of living cells.[23] Furthermore, Penedo et al. used a similar nanoprobe for 2D imaging of the actin cortical mesh by introducing it directly into living cells.[16] EBD carbon nanoprobes have the advantage of being quicker and less complex to fabricate than FIB-milled ones. Moreover, these nanoprobes can be re-grown on the same cantilever, making the cantilever reusable for routine experiments by simply growing a new nanoprobe each time.

To further enhance cell penetration efficiency with custom-designed nanoneedle probes and thereby improve intracellular AFM imaging, this study explored the resulting cell penetration force and indentation length using carbon nanoprobes fabricated by the EBD technique, compared to FIB-milled ones,[20] while also investigating the optimal tip velocity and AFM operation mode for intracellular measurements.

2. Materials and methods

2.1 Cell culture

HeLa cells (Japanese Collection of Research Bioresource) used for the experiment were cultured in Dulbecco's modified Eagle's medium (DMEM, Fujifilm Wako Pure Chemical Corporation), supplemented with 10% fetal bovine serum (FBS, Biosera) and 1% penicillin–streptomycin solution (PS, Fujifilm Wako Pure Chemical Corporation). 24 hours before the measurements, cells were detached from a Petri dish with 0.05% trypsin/EDTA for 2 minutes at 37 °C and collected by centrifuging at 1400 rpm for 3 minutes. Then, the cells were

seeded onto a 35 mm plastic cell culture dish (TPP, Techno Plastic Products AG), and cultured with DMEM with 10% FBS and 1% PS for 1 day. Before the measurements, the cell culture medium (DMEM) was replaced with Leibovitz L-15 buffer (Fujifilm Wako Pure Chemical Corporation), supplemented with a 5% PS, to maintain the condition of the cells without CO_2 equilibration. The plastic dish was placed on the JPK dish heater and maintained at 37 °C.

2.2 AFM carbon nanoprobe

The commercial Olympus BL-AC40TS cantilever (length 40 μm, spring constant 0.1 N m^{-1}) was used to fabricate a carbon nanoprobe by the EBD technique with a Helios G4 CX dual beam system (FEI, Thermo Fisher Scientific, USA). First, the very end of the triangular silicon tip was milled by FIB to make the surface flat to fabricate the EBD nanoprobe. Then, the gas source was injected using a gas injection system (GIS), with naphthalene ($C_{10}H_8$) as a gas precursor. The electron beam acceleration voltage was set at 15 kV, the current at 0.17 nA, and the working distance at 4.1 mm. The time of the gas deposition varies depending on the length and size of the required nanoprobe. Before fabrication, a layer of carbon was deposited to enhance the adhesion between the nanoprobe and the previously milled area of the original tip that came with the cantilever. The cantilever was tilted 10° for the fabrication with respect to the central axis to compensate for the mounting angle of the AFM cantilever holder. After each experiment, we inspected the nanoprobe to ensure it remains intact and retains its sharpness. If needed, a new carbon nanoprobe can be grown by removing the old one by FIB, allowing us to reuse the same cantilever routinely. It should be noted that tipless cantilevers can be used to directly grow EBD nanoprobes, eliminating the need for prior FIB usage. However, reusing the same cantilever for multiple experiments makes it impractical, as removing the previous nanoprobe can damage the cantilever surface. Therefore, using a cantilever with a tip is recommended, as it allows for the regrowth of a new EBD nanoprobe on the same cantilever by removing a portion of the cantilever tip with FIB each time without compromising the cantilever surface.

2.3 AFM cell penetration experiments

A JPK Nanowizard 4 (Bruker Nano GmbH, Berlin, Germany) microscope was used to perform the cell penetration experiments, as described previously.[20] The sensitivity and stiffness of the cantilever were calibrated by the thermal noise method implemented in the JPK AFM control software. The cantilever was positioned at the cell's periphery without interfering with the nucleus to measure the F–z curve at different modes and tip velocities. The tip was inserted into living cells at a certain speed, recording the cantilever deflection during the process until a specific set point was reached, and then the nanoprobe was subsequently withdrawn at the same speed. The penetration experiments were carried out in two different ways: (1) in the static mode, the nanoprobe above the cell was vertically moved down without any oscillation until the given set point

was reached, retracting afterward and (2) in the dynamic mode, the nanoprobe was vertically moved down while simultaneously vibrating with an oscillation amplitude of around 20 nm$_{p–p}$ at its first resonance frequency (25 kHz), withdrawing once the oscillation amplitude dropped by 40%. By penetrating each cell only once, we measured more than 30 points per method and speed.

2.4 Statistical analysis

The penetration force (F_P) and indentation length (I_L) for each F–z curve were calculated using JPK analysis software, allowing to precisely determine the contact and penetration point. The statistical calculations to obtain the average, median, and minimum to the maximum range were performed on Microsoft Excel.

3. Results and discussion

To evaluate the performance of EBD based carbon nanoprobes, we have performed F–z curve measurements on HeLa cells at different vertical speeds and calculated the required F_P and I_L values. The F–z curves were obtained on the periphery of the cell, as illustrated in the schematic in Fig. 1a, to avoid the thicker nuclear region that requires a longer probe. During the experiment, we used an optical microscope to guide us to place the nanoprobe on the target cell surface (Fig. 1b). The carbon nanoprobes were fabricated on an Olympus BL-AC40TS cantilever (length 40 μm, spring constant 0.1 N m^{-1}) using the EBD technique. Two types of needle-like nanoprobes were fabricated: one with a diameter of 120 nm, as shown in Fig. 1c, similar to the previously reported FIB-milled nanoneedle for effective comparison,[20] and another one with a diameter of 80 nm (Fig. 1d). They exhibit tip radii of approximately 26 nm and 15 nm, respectively. Note that carbon nanoprobes with diameters less than 80 nm can be fragile, often making them unsuitable for intracellular measurements. The nanoprobes were approximately 4 μm in length (Fig. 1d and e), enough to reach the substrate after penetrating the cell membrane. Detailed information about the nanoprobe fabrication can be found in the Materials and methods section.

Two different AFM operational modes, static and dynamic, were used to obtain the F–z curves (Fig. 1e). In static mode, a non-vibrating cantilever moves vertically downward, penetrating the cell and retracting after reaching the surface. To explore whether oscillation during penetration offers any advantages, the cantilever was also operated in dynamic mode, where it continuously oscillates at its resonant frequency with a specific amplitude while traveling from the cell outside to the bottom dish surface (Fig. 1e, dynamic mode). In static mode, the cantilever's vertical deflection is used as a set point, while in dynamic mode, it is defined by its oscillation amplitude. A detailed schematic of cell penetration using an AFM nanoprobe is illustrated in Fig. 1f. During the approach, the force remains zero and no cantilever deflection occurs while the nanoprobe is still far from the cell, as depicted in Fig. 1f(i).
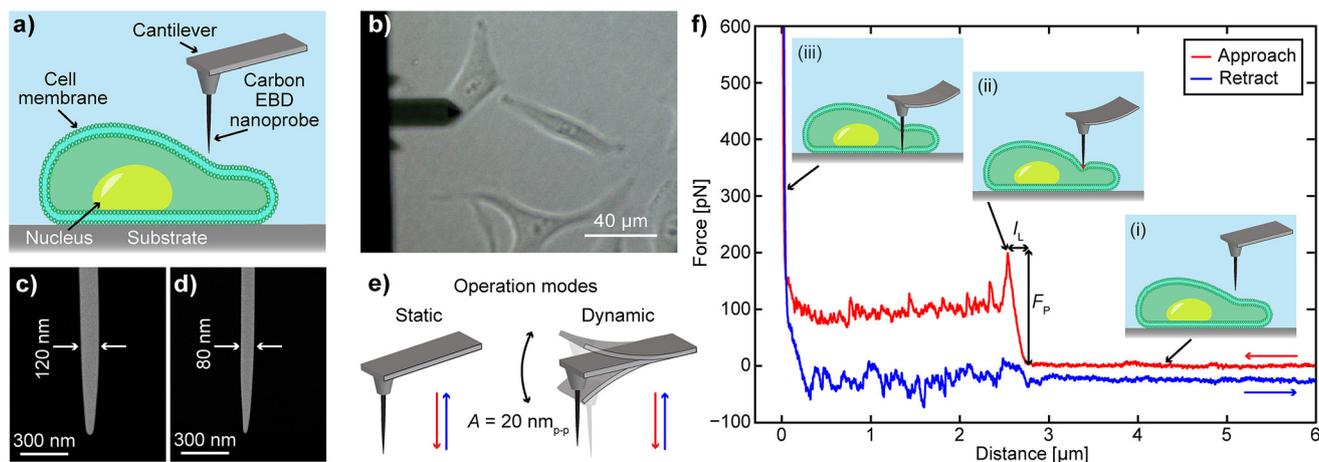
Fig. 1 (a) Schematic of the cell and AFM cantilever with an EBD-fabricated carbon nanoprobe. (b) Optical image of the cantilever positioned on a HeLa cell for $F–z$ curve measurements using EBD carbon nanoprobes with diameters of (c) 120 nm and (d) 80 nm, operating in different AFM modes: static and dynamic (e). (f) Detailed schematic of the AFM nanoprobe performing an $F–z$ curve measurement on the cell: (i) No vertical force is detected when the nanoprobe is far from the cell. (ii) As the nanoprobe makes contact and indents to penetrate the cell membrane, the cantilever vertical force increases until membrane penetration, where a sudden force drop is observed. (iii) The nanoprobe continues toward the substrate, showing a sharp rise in force, followed by retraction, as indicated by the blue line.

When the nanoprobe contacts the cell membrane and continues downward, the cantilever bends (Fig. 1f(ii)), increasing the vertical force required for penetration. Upon membrane penetration, there is a sudden drop in the vertical force and deflection. The vertical distance from the initial contact point to this sudden force drop is termed I_L, and the reached force right before the cell penetration is described as F_P. Subsequently, the nanoprobe is moved further downward and reaches the substrate, where a sharp increase in vertical force is observed (Fig. 1f(iii)). Finally, the nanoprobe retracts completely from the cell, as shown by the blue curve. In dynamic mode, the cantilever vertically goes down while continuously vibrating with an oscillation amplitude of 20 $nm_{p–p}$. When this amplitude decreases by 40% (set point), the cantilever retracts from the cell. To validate the nanoprobe's penetration of the cell membrane, we conducted a confocal microscopy experiment, as demonstrated in ESI Fig. S1.† In this experiment, both the cell membrane and the nanoprobe were stained. The $F–z$ curve obtained during confocal imaging exhibited similar characteristics, confirming the successful penetration.

To investigate the impact of the nanoprobe traveling speed on cell disturbance, we conducted cell penetration experiments at speeds of 5 μm s⁻¹, 10 μm s⁻¹, and 30 μm s⁻¹. The penetration of the cell membrane is indicated by a sharp drop in vertical force in the approach curve. In contrast, if no penetration occurs, the force increases steadily until the nanoprobe contacts the surface, at which point a sharp rise in force has occurred. Examples of $F–z$ curves at different speeds are shown in Fig. 2. The nanoprobe successfully penetrates the cell membrane at approach speeds of 5 μm s⁻¹, 10 μm s⁻¹, and 30 μm s⁻¹ (Fig. 2a–c), as indicated by a sharp drop in the vertical force. We also attempted a higher speed of 90 μm s⁻¹ (Fig. 2d), but the nanoprobe failed to penetrate and instead significantly
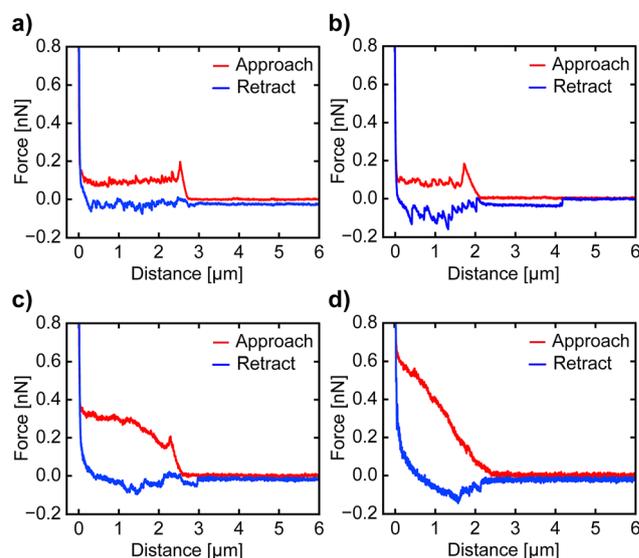
Fig. 2 Example of $F–z$ curves obtained at different approach speeds: (a) 5 μm s⁻¹, (b) 10 μm s⁻¹, (c) 30 μm s⁻¹, and (d) 90 μm s⁻¹. At 5, 10, and 30 μm s⁻¹, the nanoprobe penetrates the cell membrane, as indicated by a drop in the vertical force after contacting the cell surface. At 90 μm s⁻¹, the nanoprobe fails to penetrate, with the force continuously increasing until it reaches the substrate.

dragged the membrane. Although some $F–z$ curves at this speed show slight drops in vertical force, interpreting these curves remains challenging due to the dragging effect. Thus, we only calculate the F_P and I_L values of the $F–z$ curves obtained with speeds of 5 μm s⁻¹, 10 μm s⁻¹ and 30 μm s⁻¹ to examine the relationship between speed and cell membrane compromise or disturbance. A single $F–z$ curve was recorded

per cell to avoid the influence of the cell's reaction to damage in the measurements. The optical images of the cells after penetration show no significant changes, as depicted in ESI Fig. S2 and S3.† Before proceeding with the analysis of the recorded F–z curves, we examined the nanoprobe using SEM to confirm that its apex remained intact, maintaining its original shape and sharpness (Fig. S4 and S5†), as it is crucial for calculating the F_P and I_L values of the cell membrane.

The experimental results are shown in Fig. 3, with the statistical values summarized in Table 1, alongside the results of the FIB-milled nanoprobe from a previous study[20] for comparison. The carbon nanoprobes successfully penetrate the cell membrane, showing a 100% success rate under every condition. For the 120 nm diameter nanoprobes, lower F_P values were observed at a tip velocity of 10 μm s^{-1} (average 78 pN in static and 86 pN in dynamic mode), while higher values were recorded at 30 μm s^{-1}. At 10 μm s^{-1}, the F_P required for the

FIB-milled nanoprobe was nearly double (average 150 pN in static and 230 pN in dynamic mode) compared to the carbon nanoprobe, as detailed in Table 1. Additionally, at 10 μm s^{-1}, the F_P values for the carbon nanoprobe were more concentrated around their average value, showing less variability compared to others, as illustrated in Fig. 3a. When the diameter of the carbon nanoprobe was reduced to 80 nm, the F_P values decreased further. It shows a similar trend to the case of 120 nm diameter carbon nanoprobes, with lower F_P values observed at 10 μm s^{-1}. The average F_P values decreased by a factor of two in both static (48 pN) and dynamic (34 pN) modes compared to the 120 nm diameter carbon nanoprobe, effectively reducing the cell disturbance with a thinner nanoprobe.

For the 120 nm carbon nanoprobe, the I_L values ranged from 240 nm to 334 nm at various speeds, with lower values observed at 5 μm s^{-1} (240 nm in static mode and 254 nm in
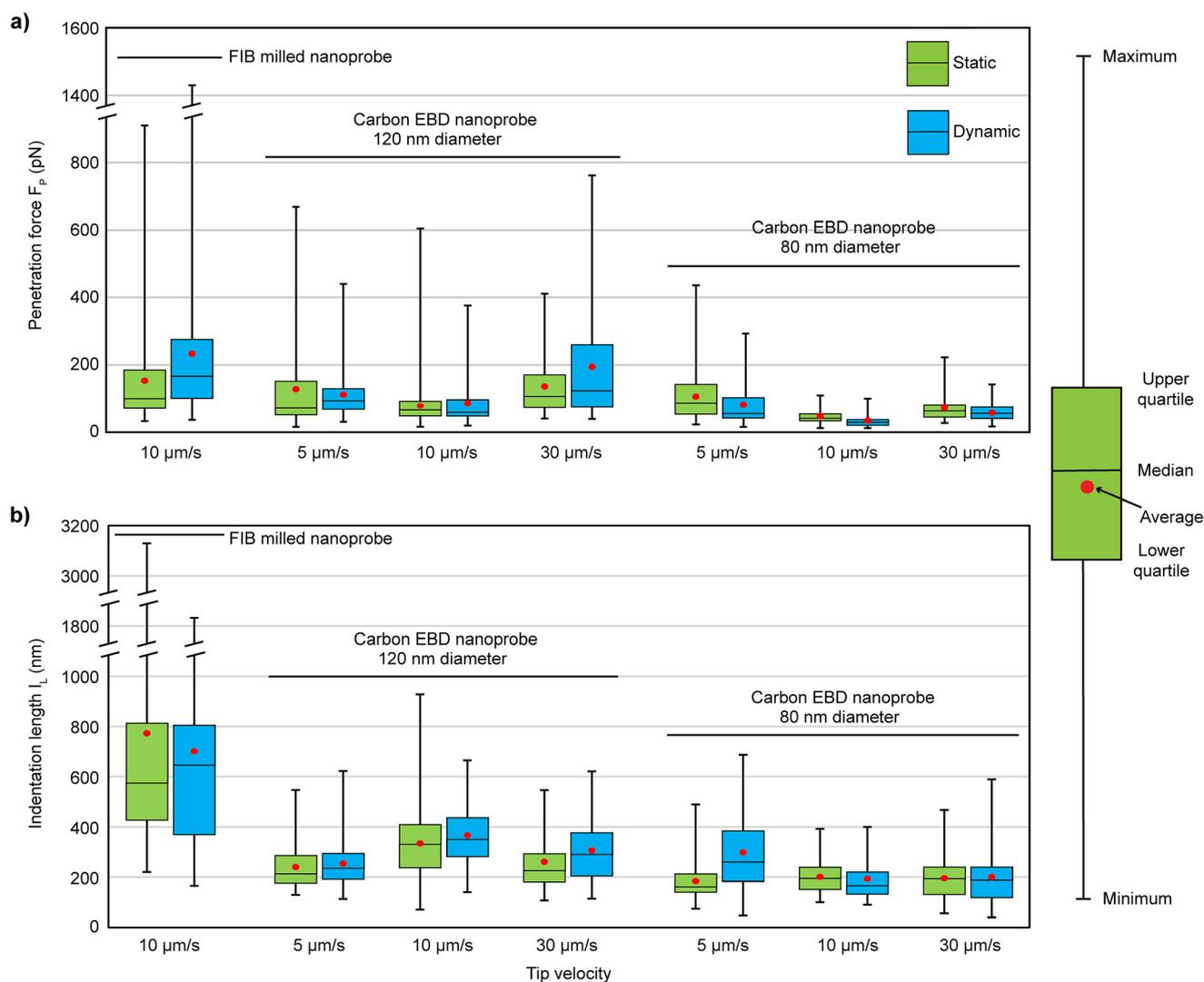

Fig. 3 Overview of results for the (a) penetration force (F_P) and (b) indentation length (I_L) of carbon EBD nanoprobes compared to FIB-milled nanoprobes from a previous study,[20] measured at different approach speeds and in different operational modes.

Table 1 Statistical data of the experiments with EBD carbon nanoprobes in this study and FIB-milled nanoprobes in the previous study[20]

Nanoprobe type	Tip speed	Operation modes	Probability [%] (success/total)	Average F_P (pN)	Median F_P (pN)	Average I_L (nm)	Median I_L (nm)
FIB milled nanoprobe[20]	10 μm s^{-1}	Static	98 (48/49)	150 ± 150	100	770 ± 600	575
		Dynamic	98 (50/51)	230 ± 240	170	700 ± 410	645
Carbon EBD nanoprobe 120 nm diameter	5 μm s^{-1}	Static	100 (101/101)	127 ± 127	72	**240 ± 89**	**213**
		Dynamic	100 (85/85)	111 ± 70	93	254 ± 91	235
	10 μm s^{-1}	Static	100(99/99)	**78 ± 66**	65	334 ± 148	330
		Dynamic	100 (53/53)	86 ± 70	**59**	316 ± 146	291
	30 μm s^{-1}	Static	100 (46/46)	135 ± 86	106	265 ± 110	226
		Dynamic	100 (44/44)	194 ± 170	123	305 ± 116	289
Carbon EBD nanoprobe 80 nm diameter	5 μm s^{-1}	Static	100 (35/35)	106 ± 78	86	**183 ± 90**	**161**
		Dynamic	100 (33/33)	81 ± 67	55	298 ± 156	260
	10 μm s^{-1}	Static	100 (42/42)	48 ± 23	41	200 ± 66	195
		Dynamic	100 (33/33)	**34 ± 22**	**29**	193 ± 83	165
	30 μm s^{-1}	Static	100 (35/35)	68 ± 46	57	195 ± 83	194
		Dynamic	100 (41/41)	57 ± 26	56	199 ± 117	188

dynamic mode), as shown in Table 1. In comparison, the FIB-milled nanoprobe exhibited significantly larger I_L values, averaging 770 nm in static mode and 700 nm in dynamic mode.[20] Notably, with the carbon nanoprobe, the I_L value decreased by half, and the values were more consistently clustered around the average, whereas the FIB-milled data showed much higher variability, with deviations of 600 nm in static mode and 410 nm in dynamic mode. When the carbon nanoprobe diameter was reduced to 80 nm, the I_L value further decreased, ranging from 183 nm to 298 nm, as shown in Table 1. The I_L values were relatively stable across different speeds, showing minimal variation except at 5 μm s^{-1} in dynamic mode, where the average I_L value increased to 298 nm. This indicates that reducing the nanoprobe's diameter significantly reduces the overall membrane deformation. Finally, it was found that the 80 nm diameter carbon nanoprobe, at a speed of 10 μm s^{-1}, caused less cell disturbance as it required lower F_P (34 pN) and I_L (193 nm) values during penetration. The speed of 10 μm s^{-1} not only increased the penetration efficiency but also caused less perturbation to the cells during penetrations.

By reducing the diameter of the carbon nanoprobe from 120 nm to 80 nm, we achieved a significant reduction in both F_P and I_L values during penetration. Despite having similar diameters, the 120 nm EBD fabricated carbon nanoprobe consistently showed less cell membrane disturbance compared to the FIB-milled nanoprobe.[20]

To further understand this discrepancy, we examined the TEM images of the nanoprobes' apex (Fig. 4). The typical apex radius of an FIB-milled nanoprobe is approximately 50 nm, as shown in Fig. 4a. In contrast, the 120 nm base diameter carbon nanoprobe fabricated *via* EBD has an apex radius of 26 nm, roughly half that of the FIB-milled nanoprobe, as depicted in Fig. 4b. This sharper apex contributes to the reduction in the F_P and I_L values during cell penetration experiments. Moreover, the apex radius is further reduced to 15 nm in the 80 nm diameter nanoprobe, highlighting the superior precision of the EBD technique. In com-

parison, further reduction of the apex radius using the FIB milling technique proves challenging, as attempts to achieve smaller radii can result in the collapse of the entire nanoprobe.

Moreover, in this study, the SEM images of EBD carbon nanoprobes taken before and after the cell penetration experiments confirm that the nanoprobe's apex remained unchanged across all conditions (ESI Fig. S4 and S5†), which suggests that there is no influence of contamination or cell debris in the measurement of F_P and I_L values of the cell membrane. Although, in a few nanoprobes, a small amount of cell debris was adsorbed on the side wall during measurement, no correlation was found between these contaminations and the cell penetration techniques (static and dynamic) or tip velocities (5 μm s^{-1}, 10 μm s^{-1}, and 30 μm s^{-1}).

Another key difference between the FIB-milled nanoprobe from previous studies[20] and the EBD fabricated nanoprobe in this study lies in their surface properties: the former is hydrophilic (silicon), while the latter is hydrophobic (carbon). Both experimental and theoretical research studies have explored the effect of tip surface properties during cell membrane penetration,[24–27] but results remain inconclusive. In experimental works, Schneider *et al.* found that hydrophobic tips required less F_P to penetrate lipid bilayers compared to hydrophilic ones,[24] while Angle *et al.* reported no significant difference in F_P between chemically modified hydrophobic and hydrophilic tips.[25] On the theoretical side, studies suggest that hydrophobic probes cause more disturbance when penetrating lipid bilayers.[26,27] However, in this study, the hydrophobic carbon nanoprobe showed no significant issues during membrane penetration, with $F-z$ curves looking similar to those of the hydrophilic silicon nanoprobe from previous work.[20] Moreover, to understand the effect of surface properties in the retraction process, we calculated the root-mean-square amplitude (F_{rms}) of the retraction $F-z$ profile under the baseline, where no significant differences were observed between the hydrophilic silicon and hydrophobic carbon nanoprobes
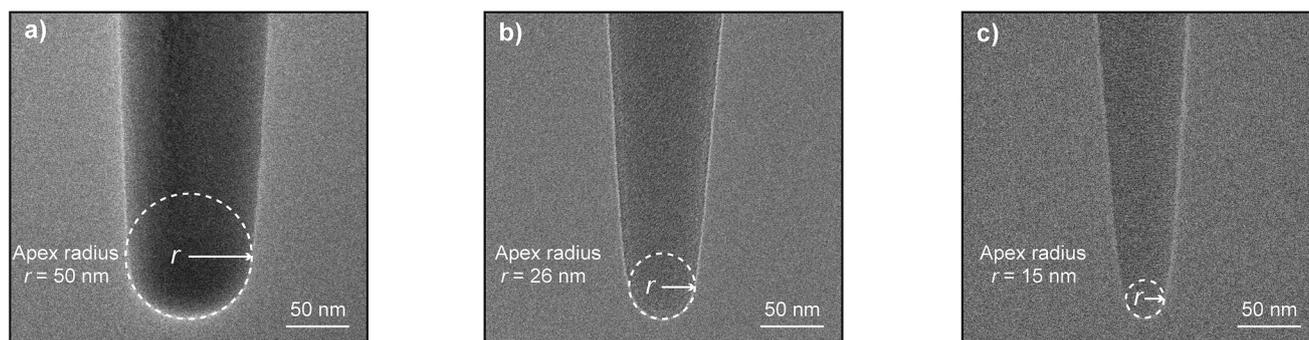
Fig. 4 TEM images of the nanoprobes' apex, (a) FIB-milled nanoprobe (r = 50 nm), (b) 120 nm carbon EBD nanoprobe (r = 26 nm) and (c) 80 nm carbon EBD nanoprobe (r = 15 nm).

(Fig. S6 and Table S1†). Additionally, the hydrophobic nanoprobe caused less cellular damage, reducing F_P and I_L during penetration, likely due to its sharper tip apex, as illustrated in Fig. 4. This suggests that membrane penetration is more influenced by tip sharpness than surface properties.

Cell penetration experiments were conducted in both static and dynamic modes. Interestingly, the results showed no significant differences in F_P and I_L between the two modes (Fig. 3), suggesting that cantilever oscillation in dynamic mode may not offer any distinct advantage. However, our recent 3D-AFM study on suspended nanostructures found large vertical force offset in F–z curves during static mode measurements, indicating strong lateral friction between the nanoprobe wall and the CNT fiber, which was significantly reduced by oscillating the nanoprobe in dynamic mode.[28] Inspired by these findings, we calculated the vertical force offsets from the F–z curves at different approach speeds obtained by FIB-milled and EBD carbon nanoprobes (Fig. 5) to investigate whether lateral friction between the nanoprobe walls and the upper cell membrane (which corresponds to that vertical force offset) varies between static and dynamic modes after penetration. The force offset was determined as the difference between the baseline and the point where the cantilever's vertical force drops after penetration, as illustrated in Fig. 5a. The overall results are displayed in Fig. 5b, with a summary of the statistical values provided in Table S2 (see the ESI†).

For the FIB-milled nanoprobe, the force offset was higher in static mode compared to dynamic mode (average 95 pN in static and 78 pN in dynamic mode). A similar pattern was seen with both carbon EBD nanoprobes, where static mode consistently showed higher force offsets across all speeds (Fig. 5b). For the 120 nm diameter carbon nanoprobe in dynamic mode, the lowest force offset was observed at 10 μm s⁻¹ (59 pN), while the highest was at 30 μm s⁻¹ (176 pN) (Table S2†). This force offset was further decreased with the 80 nm carbon nanoprobe. Notably, at 10 μm s⁻¹ in dynamic mode, the force offset was very low, averaging 15 pN, and in some cases, nearly zero. Although the differences between 5 μm s⁻¹ and 10 μm s⁻¹ in dynamic mode were minimal, friction at 30 μm s⁻¹ was significantly higher, with the vertical force not decreasing substantially after membrane penetration for both EBD carbon nanoprobes. Therefore, oscillating the cantilever in dynamic mode reduces friction between the nanoprobe wall and the cell membrane, thereby minimizing potential cell disturbance. Additionally, the cantilever's approaching speed influences friction; specifically, a speed of 10 μm s⁻¹ yields the lowest friction, improving the efficiency of intracellular measurements and reducing potential damage to the cell.
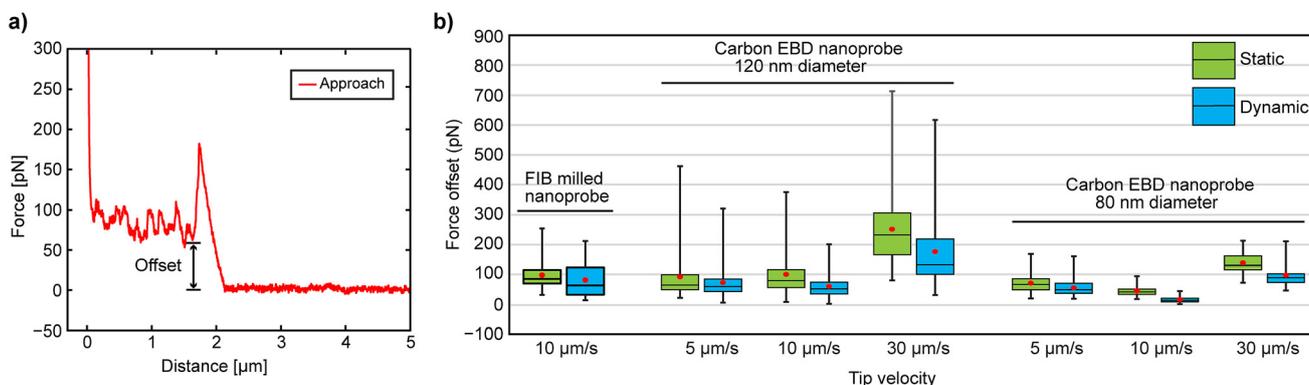
Fig. 5 (a) Force offset analysis from F–z curves. (b) Results of the offset measurement from F–z curves obtained at different speeds by using different methods with FIB-milled[20] and EBD nanoprobes.

4. Conclusions

In this study, we investigated the required cell penetration force and indentation length using carbon nanoprobes fabricated by the EBD technique, while also examining the optimal tip velocity and AFM operation mode for intracellular measurements. Our experiments revealed that EBD-fabricated 120 nm diameter carbon nanoprobes significantly reduce the F_P and I_L compared to the similar diameter FIB-milled nanoprobes (Table 1). This improvement is attributed to the sharper tip ends achievable by the EBD technique (Fig. 4). Further reduction in the probe diameter and tip sharpness (80 nm and 15 nm, respectively) resulted in even lower F_P and I_L. The minimum F_P observed with an 80 nm diameter nanoprobe was, on average, 34 pN. Further reduction in the diameter might lower F_P, but thinner nanoprobes are more likely to break or bend during measurement due to the high aspect ratio of the nanoprobes. This finding has important implications for minimizing cell membrane disturbance and cellular damage during nanoprobe insertion. Additionally, while previous studies present contradictory results regarding the impact of tip hydrophobicity on penetration forces, our experiments show no significant differences when penetrating cell membranes with hydrophobic carbon nanoprobes. However, a more systematic investigation is needed to fully understand the impact of surface properties on cell penetration.

The penetration experiments with varying approaching speeds revealed that at a higher speed of 90 μm s^{-1}, the nanoprobe was unable to successfully penetrate the cell membrane (Fig. 2). Notably, a speed of 10 μm s^{-1} proved to be optimal, as it resulted in lower F_P and I_L, therefore reducing cell disturbance (Fig. 3). At a slower speed of 5 μm s^{-1}, the nanoprobe causes more membrane disturbance, likely due to prolonged stress from the slower interaction. In contrast, at 30 μm s^{-1} the membrane may exhibit increased stiffness due to the faster indentation speed, necessitating greater force for penetration and resulting in additional cell disturbance. To make the measurement faster, one option is to increase the retraction speed relative to the approaching speed, using the approach portion of the curve to extract the cell structural information. Furthermore, oscillating the nanoprobe in dynamic mode reduces the lateral friction between the nanoprobe and the cell membrane during F–z curve measurements, compared to the static mode. This decreased friction minimizes membrane dragging and thus potential damage, which is crucial for intracellular 3D-AFM imaging of living cells, where the nanoprobe repeatedly penetrates the cell membrane for obtaining the required multiple F–z curves for 3D reconstruction. The findings in this study are not specific to HeLa cells as our experience suggests that these results are likely consistent across various cell types. However, a systematic investigation with other cell lines is required for a more quantitative understanding. The results presented here will greatly help refine the intracellular measurement techniques in terms of speed, spatial resolution and reduced cell perturbation and damage.

Author contributions

M. S. A.: data curation, formal analysis, investigation, visualization, writing original draft and editing; M. P.: conceptualization, supervision, validation, and writing – review and editing; T. I.: methodology; M. M. H.: resources; K. M.: resources; K. M.: data curation; T. F.: conceptualization, funding acquisition, supervision, validation, and writing – review and editing.

Data availability

Data for this article, including raw data for the graphs in Fig. 1f, 2, 3 and 5, are available at GitHub at **https://github.com/fukuma-lab/cell-penetration-paper**.

Conflicts of interest

There are no conflicts to declare.

Acknowledgements

References

1 J. Hu, M. Gao, Z. Wang and Y. Chen, *Micron*, 2022, **159**, 103293.

2 Y. F. Dufrêne, A. Viljoen, J. Mignolet and M. Mathelié-Guinlet, *Cell. Microbiol.*, 2021, **23**, e13324.

3 E. Moeendarbary, I. P. Weber, G. K. Sheridan, D. E. Koser, S. Soleman, B. Haenzi, E. J. Bradbury, J. Fawcett and K. Franze, *Nat. Commun.*, 2017, **8**, 14787.

4 A. Levillain, C. B. Confavreux, M. Decaussin-Petrucci, E. Durieux, P. Paparel, K. L. B. Carval, L. Maillard, F. Bermond, D. Mitton and H. Follet, *Materialia*, 2022, **25**, 101555.

5 A. Massey, J. Stewart, C. Smith, C. Parvini, M. McCormick, K. Do and A. X. Cartagena-Rivera, *Nat. Rev. Phys.*, 2024, **6**, 269–282.

6 S. E. Cross, Y. S. Jin, J. Rao and J. K. Gimzewski, *Nat. Nanotechnol.*, 2007, **2**, 780–783.

7 N. Kodera, D. Yamamoto, R. Ishikawa and T. Ando, *Nature*, 2010, **468**, 72–76.

8 T. Osada, H. Uehara, H. Kim and A. Ikai, *J. Nanobiotechnol.*, 2003, **1**, 1–8.

9 H. Uehara, T. Osada and A. Ikai, *Ultramicroscopy*, 2004, **100**, 197–201.

10 J. Liu, J. Wen, Z. Zhang, H. Liu and Y. Sun, *Microsyst. Nanoeng.*, 2015, **1**, 1–15.

11 Y. R. Silberberg, S. Mieda, Y. Amemiya, T. Sato, T. Kihara, N. Nakamura, K. Fukazawa, K. Ishihara, J. Miyake and C. Nakamura, *Biosens. Bioelectron.*, 2013, **40**, 3–9.

12 Y. R. Silberberg, R. Kawamura, S. Ryu, K. Fukazawa, K. Ishihara and C. Nakamura, *J. Biosci. Bioeng.*, 2014, **117**, 107–112.

13 S. W. Han, C. Nakamura, I. Obataya, N. Nakamura and J. Miyake, *Biochem. Biophys. Res. Commun.*, 2005, **332**, 633–639.

14 H. Liu, J. Wen, Y. Xiao, J. Liu, S. Hopyan, M. Radisic, C. A. Simmons and Y. Sun, *ACS Nano*, 2014, **8**, 3821–3828.

15 K. P. McCreery, X. Xu, A. K. Scott, A. K. Fajrial, S. Calve, X. Ding and C. P. Neu, *Small*, 2021, **17**, 2006699.

16 M. Penedo, K. Miyazawa, N. Okano, H. Furusho, T. Ichikawa, M. S. Alam, K. Miyata, C. Nakamura and T. Fukuma, *Sci. Adv.*, 2021, **7**, eabj4990.

17 T. Ichikawa, M. S. Alam, M. Penedo, K. Matsumoto, S. Fujita, K. Miyazawa, H. Furusho, K. Miyata, C. Nakamura and T. Fukuma, *STAR Protoc.*, 2023, **4**, 102468.

18 I. Obataya, C. Nakamura, S. W. Han, N. Nakamura and J. Miyake, *Biosens. Bioelectron.*, 2005, **20**, 1652–1655.

19 S. W. Han, S. Ryu, T. Kitagawa, H. Uetsuka, N. Fujimori, Y. Aoki, R. Ota, Y. Amemiya, N. Shimamoto, C. Nakamura and J. Miyake, *Arch. Histol. Cytol.*, 2009, **72**, 261–270.

20 M. Penedo, T. Shirokawa, M. S. Alam, K. Miyazawa, T. Ichikawa, N. Okano, H. Furusho, C. Nakamura and T. Fukuma, *Sci. Rep.*, 2021, **11**, 7756.

21 R. Kawamura, K. Shimizu, Y. Matsumoto, A. Yamagishi, Y. R. Silberberg, M. Iijima, S. Kuroda, K. Fukazawa, K. Ishihara and C. Nakamura, *J. Nanobiotechnol.*, 2016, **14**, 1–9.

22 T. Uchihashi, N. Kodera and T. Ando, *Nat. Protoc.*, 2012, **7**, 1193–1206.

23 M. Shibata, T. Uchihashi, T. Ando and R. Yasuda, *Sci. Rep.*, 2015, **5**, 1–7.

24 J. Schneider, W. Barger and G. U. Lee, *Langmuir*, 2003, **19**, 1899–1907.

25 M. R. Angle, A. Wang, A. Thomas, A. T. Schaefer and N. A. Melosh, *Biophys. J.*, 2014, **107**, 2091–2100.

26 K. Lv and Y. Li, *Langmuir*, 2018, **34**, 7681–7689.

27 F. Liu, D. Wu, R. D. Kamm and K. Chen, *Biochim. Biophys. Acta, Biomembr.*, 2013, **1828**, 1667–1673.

28 M. S. Alam, M. Penedo, T. Sumikama, K. Miyazawa, K. Hirahara and T. Fukuma, *Small Methods*, 2024, 2400287.